Welding in the World (2024) 68:2511–2520
https://doi.org/10.1007/s40194-024-01785-7

RESEARCH PAPER

Microstructures and mechanical properties of TiAl joint brazed with Ti-Mn-Fe-Ni-Zr system medium-entropy filler alloy

Zhiliang Zhai[1] · Xinyu Ren[1] · Yonglai Shang[1] · Yaoyong Cheng[1] · Haishui Ren[1] · Huaping Xiong[1] · Yongjuan Jing[1]

Received: 11 December 2023 / Accepted: 7 May 2024 / Published online: 25 May 2024

Abstract

A five-element medium-entropy filler alloy with composition of Ti-(18 ~ 24)Mn-(12 ~ 18)Fe-(3 ~ 8)Ni-(3 ~ 8)Zr (wt.%) was proposed for vacuum brazing of TiAl-based alloy. The filler alloy was mainly composed of Ti-based solid solution and Ti-(Fe, Mn) compound dissolved with elements of Ni and Zr. The filler alloy ingot was ground into powder and then the filler powder was preset into the V-shaped groove butt joint with a gap of 50 μm. The Ti-Mn-Fe-Ni-Zr brazing alloy showed the liquidus temperature of 1060.1 °C, and also presented excellent wettability on TiAl substrate at 1110 °C for 10 min. The brazed joint mainly consisted of γ-TiAl, α_2-Ti_3Al, and residual brazing filler reaction phase. The brazing condition of 1210 °C/45 min exhibited the maximum joint thickness of 308 μm and the maximum area percentage of γ-TiAl phase of 33.77%, with almost elimination of residual brazing filler reaction phase within the joint, and meanwhile offered the maximum room-temperature tensile strength of 418 MPa, 70.85% of the base alloy. The joint fracture showed a mixed mode of intergranular and transgranular fracture.

Keywords TiAl alloy · Medium-entropy alloy · Brazed joint · Microstructure · Tensile strength

1 Introduction

For the purpose of energy savings and emission reductions, developing high-performance materials in terms of thermo-mechanical properties is needed for air-transport industry [1]. TiAl-based alloys are considered to be really attractive for high-temperature applications owing to their low density, high specific modulus, and mechanical strength [2], acceptable creep behavior and good oxidation resistance [3]. From the perspective of weight reduction, TiAl-based alloys are superior to Ni-based superalloys [4]. However, one challenge is that TiAl-based alloys are subjected to the poor weldability and machinability, which is not beneficial to practical application [5].

Appropriate joining technologies for TiAl-based alloys are urgently required to expand their applications, including the joining of different TiAl components and the repair of TiAl castings. Brazing technique has been proved effective as a unique joining process for releasing the residual stress and avoiding cracks to a certain extent [6]. Recently, progress in brazing process such as friction stir vibration brazing (FSVB) provides a new insight to enhance the metallurgy reaction between the brazing seam and the base metal [7]. In general, a sound brazing joint could be achieved by design of the filler alloy with suitable composition [8], optimizing brazing parameter [9] as well as controlling brazing process [10].

Although Ag-based brazing filler alloy could braze TiAl alloy successfully, the joint suffers from

Highlights

- A 5-element medium-entropy brazing filler alloy with Ti-Mn-Fe-Ni-Zr composition system was proposed for joining TiAl-based alloy and microstructures and mechanical properties of the TiAl brazed joint were studied.
- The brazing parameters had an evident effect on the joint thickness, the area percentage of γ-TiAl phase within the joint and the thickness of residual brazing filler reaction phase, as well as the fracture location.
- Under the brazing condition of 1210 °C/45 min, the brazed joint exhibited the maximum tensile strength of 418 MPa at room temperature, corresponding to the highest joint strength coefficient of 70.85%.

✉ Haishui Ren
seawater2011@163.com

✉ Huaping Xiong
xionghp69@163.com; xiaonghuaping69@sina.cn

[1] Welding and Plastic Forming Division, Beijing Institute of Aeronautical Materials, Beijing 100095, People's Republic of China

insufficient bonding strength. For instance, within TiAl intermetallic joints brazed with BAg-8 [11], the formation and excessive growth of brittle Al-Cu-Ti reaction layer would deteriorate the joint properties, especially at high temperatures. Compared with Ag-based brazing alloy, Ti-based brazing alloy used to join TiAl-based alloy could represent high bonding strength. For example, the joint brazed by Ti-Zr-Cu-Ni-Co [12] filler showed a relatively high tensile strength at room temperature, which was up to 316 MPa. But brittle phases at the joint interface suppressed the improvement of joint strength.

For solving the joining challenges of the advanced TiAl material, it is of great importance to search for new joining filler alloys [13]. In our previous studies, brazing filler alloys of Ti-Zr-Fe [14, 15], Ti-Ni-Nb-Zr [16, 17], and Ti-Zr-Cu-Ni [18] were proposed for TiAl brazing. However, the concentration of Zr element within the brazing fillers should be strictly limited to 8 ~ 11 wt.% [19] for sufficient diffusion. Differently, Fe element was demonstrated not only possessing excellent diffusion rate but also accelerating self-diffusion rate in α-Ti [20]. More importantly, certain amounts of Fe [21] and Mn [22] were added in TiAl alloy for solid solution strengthening, based on the Ti-Mn-Fe ternary system [23]. To decrease the melting point of the filler alloy, another Ni-Zr binary alloy with a certain percentage was added based on Ni-Zr [24] binary eutectic compositions. With the design concept of multi-principal element alloys (MPEAs) [25, 26], in this paper, a 5-element medium-entropy brazing filler alloy with Ti-Mn-Fe-Ni-Zr composition system was thus designed for TiAl joining.

The joining of TiAl alloy was attempted by using the newly developed 5-element medium-entropy brazing filler alloy, and the aim of this study was to verify the feasibility of using the new system filler alloy to achieve high joint strength. The detailed compositions and phases across the brazed joint were analyzed. Additionally, interfacial microstructures and mechanical properties of the brazed joint were investigated. Room-temperature tensile test was performed to evaluate the joint performance, and the joining mechanism was discussed.

2 Experimental procedures

The nominal composition of TiAl intermetallic was Ti-46Al-(3 ~ 4)Nb-(2 ~ 3)(Cr, Ta, B) (at.%), which was fabricated by vacuum arc remelting and thermo-mechanical treatment. The Ti-(18 ~ 24)Mn-(12 ~ 18)Fe-(3 ~ 8)Ni-(3 ~ 8)Zr (wt.%) filler alloy ingot was fabricated by arc melting technique in high purity argon gas atmosphere. The cast ingot was broken down into pieces and subsequently ground into powder. Then, the particles were preset into the 90° V-shaped groove butt joint with a narrow assembly gap of 50 μm, as shown in Fig. 1a.

The TiAl alloy was cut into specimens with the size of 9 mm × 11 mm × 18 mm. Prior to brazing experiment, the sample surfaces to be joined were polished by SiC grit paper and then ultrasonically cleaned for 15 min in ethyl alcohol solutions. The brazing experiments were carried out in a vacuum brazing furnace, with a high vacuum of 5×10^{-3} Pa to 9×10^{-3} Pa. The brazing temperature varied from 1140 to 1210 °C, which was higher than the liquidus temperature of filler alloy. On this basis, not only the weak brazing parameters of 1140 °C/20 min but also the strong brazing parameters such as 1180 °C/75 min or 1210 °C/45 min were chosen. Meanwhile, three different dwell times of 20 min, 45 min, and 75 min were selected. Based on the geometric dimensions for plates in Fig. 1b, joint specimens with a joining area of (1.0 ~ 1.5) mm × 2.5 mm were prepared for tensile test.

Differential scanning calorimetry (DSC) with a heat rate of 10 °C/min was performed to determine the thermal behavior of Ti-Mn-Fe-Ni-Zr system brazing alloy. The average contact angle on the TiAl alloy after heating at 1110 °C for 10 min in vacuum was calculated from the four measured value of the sample cross-section in vertical direction. Scanning electron microscope (SEM) equipped with an energy-dispersive X-ray spectrometer (EDS) attachment was used to observe joint microstructure. By means of phase extraction software, area percentage of γ-TiAl phases within the joint was measured. The average value was calculated by at least three different zones from the joint cross-section. Joint tensile strength was measured by a universal testing machine with a loading speed of 0.5 mm/min at room temperature, and the reported tensile strength was the average value of at least three measurements for the same brazing condition.

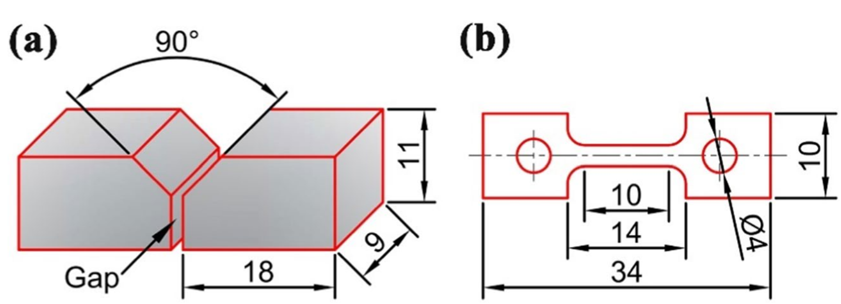

Fig. 1 Schematic of assembly specimens (**a**) and geometric dimensions (**b**)

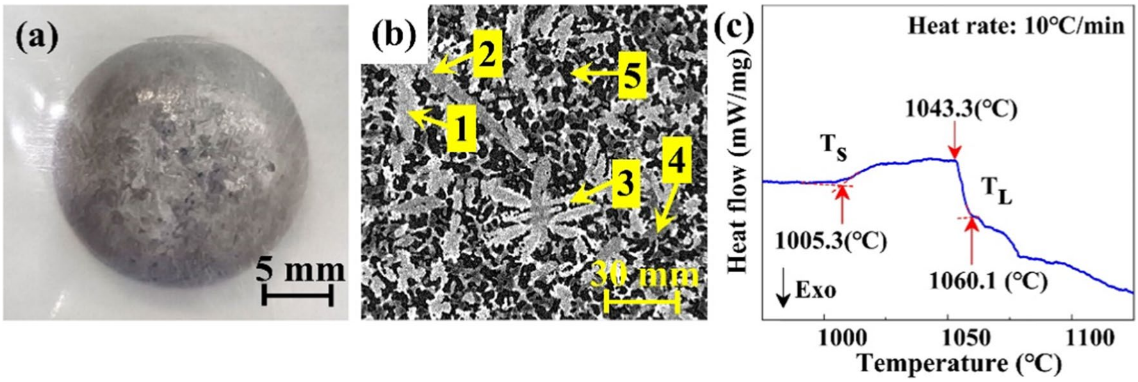

Fig. 2 Cast ingot (**a**), backscattered electron image (**a**) and DSC results (**b**) of Ti-Mn-Fe-Ni-Zr medium-entropy filler alloy

Table 1 EDS analysis results for microzones marked in Fig. 2

Microzones	Element (at.%)					Deduced phases
	Ti	Mn	Fe	Ni	Zr	
1	47.61	29.47	16.70	2.88	3.34	Ti-(Fe, Mn) compound dissolved with Ni and Zr
2	56.48	23.67	14.99	2.53	2.33	Ti-(Fe, Mn) compound + Ti-rich phases
3	57.28	19.16	12.94	5.47	5.15	Ti-(Fe, Mn) compound + Ti-rich phases
4	61.64	13.54	15.21	7.17	2.44	Ti-rich phases dissolved with Mn, Fe, Ni and Zr
5	71.32	14.07	10.33	2.86	1.42	Ti-rich phases dissolved with Mn, Fe, Ni and Zr

Table 2 Calculation results of empirical parameters for the Ti-Mn-Fe-Ni-Zr braze alloy

Alloy	T_m/K	ΔH_{mix}/ $kJ \cdot mol^{-1}$	ΔS_{mix} /$J \cdot K^{-1} \cdot mol^{-1}$	Ω	δ %
Ti-Mn-Fe-Ni-Zr	1834	−17.55	9.42	0.98	6.72

3 Results and discussion

3.1 Characteristics of Ti-Mn-Fe-Ni-Zr medium-entropy filler alloy

Figure 2a shows that the cast filler ingot and Fig. 2b shows the backscattered electron image of the 5-element medium-entropy filler alloy, and three main phases could be observed. Based on the EDS analysis results in Table 1, the filler was mainly composed of Ti-(Fe, Mn) compound dissolved with 2 ~ 4 at.% Ni and Zr (microzone “1”), and Ti-(Fe, Mn) compound and Ti-rich phases dissolved with 2 ~ 8 at.% Ni and Zr (microzone “2” and “3”), as well as Ti-rich phases dissolved with Mn, Fe, Ni, and Zr (microzone “4” and “5”) (Table 2).

The Ti-Mn-Fe alloy system exhibits good compatibility within the three elements and there is a eutectic composition of Ti-(19 ~ 25)Mn-(14 ~ 20)Fe (wt.%), with the liquidus temperature of about 1139°C [27] in this ternary alloy system. In the meantime, Ni-Zr binary eutectic composition of Ni-46.9Zr (wt.%) was also added as an effective melting point depressant with the liquidus temperature of 1061°C [24]. On this basis, it can be deduced that there might exist a 5-element eutectic composition of Ti-(18 ~ 24)Mn-(12 ~ 18)Fe-(3 ~ 8)Ni-(3 ~ 8)Zr (wt.%) with lower melting point.

According to DSC analysis results in Fig. 2c, the melting range of the filler alloy was 1005.3 ~ 1060.1 °C. Due to the fact that the liquidus temperature is lower than some reported Ti-based brazing filler alloy, such as Ti-Ni-Nb [28, 29] eutectic braze alloy and Ti-Fe-Mn [27] eutectic braze alloy, the brazing experiment could be performed at a lower brazing temperature, which might be beneficial to control the interface reaction [30].

Figure 3 presents the wettability experiment results of the novel filler on TiAl alloy at 1110 °C for 10 min. As shown in Fig. 3, the filler melted and reacted with the base metal. The contact angle on the TiAl alloy was measured as 30°. The maximum reaction layer thickness of the Ti-Mn-Fe-Ni-Zr braze alloy in the TiAl alloy was about 95 ~ 105 μm in Fig. 3b-c, which was close to that of the Fe-Ni-Co-Cr-Si-B [31] filler alloy with 110 μm at 1180 °C for 10 min. This illustrated that a stronger reaction and sufficient spreading behavior of filler still occurred with the TiAl substrate.

From the thermodynamic point of view, the empirical parameters, including four main parameters, were calculated for the Ti-Mn-Fe-Ni-Zr braze alloy to predict the phase formation in high-entropy alloys (HEAs) [32–34], as shown in Table 2. Among the four parameters, the mixing

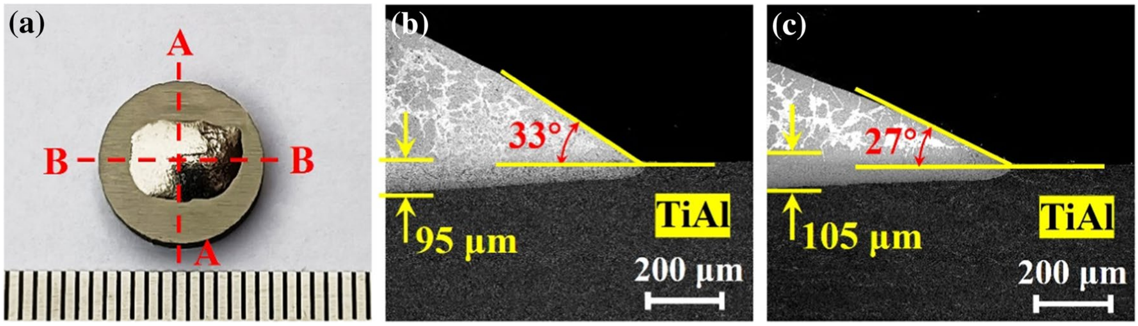

Fig. 3 Wettability of Ti-Mn-Fe-Ni-Zr filler alloy on TiAl at 1110 °C for 10 min: wetting morphology (**a**), contact angle from the cross-section of A-A (**b**) and B-B (**c**)

entropy (ΔS_{mix}) of 9.42 J·K^{-1}·mol^{-1}, the mixing enthalpy (ΔH_{mix}) of − 17.55 kJ·mol^{-1}, the parameter (Ω) of 0.98, and the atomic size difference (δ) of 6.72% were presented. Then, due to the ΔS_{mix} being between 1.0 R and 1.5 R (8.314 ~ 12.471 J·K^{-1}·mol^{-1}), the Ti-Mn-Fe-Ni-Zr filler metal should be classified as medium-entropy alloy [35].

3.2 Microstructural analysis of the brazed joints

Several choices of brazing parameters were made to join TiAl alloy at 1140 °C/20 min, 1180 °C/45 min, 1180 °C/75 min, and 1210 °C/45 min, respectively. The backscattered electron images of the TiAl joints brazed by the four different brazing parameters are shown in Fig. 4. The EDS analysis results for the typical microzones marked in Fig. 4 are displayed in Table 3.

As the typical interfacial microstructure of TiAl joint at 1140 °C/20 min, the thickness of the brazed joint reached 171 μm in Fig. 4a. The white phase (microzone "3") in the center of the brazing seam exhibited as almost continuous layer, with a thickness of 29 μm. Obviously, the quantities of gray phase (microzone "2") were far more than that of the white phase in the brazing seam. Since the composition of white phase in the brazed joint was close to that of the braze alloy, it could be identified as the residual brazing filler reaction phase. Based on the Ti-Al binary alloy phase diagram [36–38], the gray phase in the brazing seam showing a similar Ti/Al ratio to that of the parent metal might be regarded as the γ-TiAl + α_2-Ti_3Al phase [39, 40].

From the EDS analysis results shown in Table 3, except for the residual brazing filler reaction phase, generally Ti element concentration within the brazing seam was comparable to that of the parent material. Al element significantly diffused from the TiAl base metal to the brazing seam, with the concentration high up to 32.40 ~ 36.30 at.%. For microzones "3", "6," and "9" in the central part of the joint, their compositions were characterized by 29.65 ~ 31.58 at.% Ti, 34.30 ~ 40.93 at.% Al, 7.13 ~ 10.40 at.% Fe, 6.55 ~ 9.55 at.% Mn, 4.58 ~ 5.65 at.% Ni, and 5.07 ~ 6.02 at.% Zr, and thus they should be regarded as residual brazing filler reaction phase, and this was agreement with the area distribution map of elements in Fig. 5. Therefore, for eliminating the residual brazing filler reaction phase within joint, higher brazing temperature or longer dwell time is needed.

In comparison, the joint thickness was significantly increased to 258 μm and the thickness of the residual brazing filler reaction phase (microzone "6" in Fig. 4b) was sharply decreased to 14 μm by the brazing parameter of 1180 °C/45 min, as shown in Fig. 4b. But the residual brazing filler reaction phase still remained continuous. Interestingly, in this case, the dark lath-like phase (microzone "5") appeared in the brazing seam. According to the Ti-Al binary alloy phase diagram [36–38], it is reasonable to deduce the dark phase to be γ-TiAl phase [39, 40].

The Al element concentration in the brazing seam was increased to 33.45 ~ 44.12 at.%, indicating the enhanced diffusion of Al element by the brazing parameter of 1180 °C/45 min. However, the expected sufficient diffusion of elements Fe, Mn, Ni, and Zr had not been accomplished due to the presence of the residual brazing filler reaction phase. For eliminating the residual brazing filler reaction phase, it is necessary to further prolong the dwell time or increase the brazing temperature.

On the one hand, with prolonging the dwell time to 75 min at the brazing temperature of 1180°C, the joint thickness was slightly increased to 278 μm and the thickness of the residual brazing filler reaction phase (microzone "9") was decreased to only 6 μm, as shown in Fig. 4c. More importantly, the residual brazing filler reaction phase became discontinuous. It appeared that the lath-like γ-TiAl partially began to aggregate in the joint. Compared with the joint brazed at 1180 °C/45 min, the concentration of Al element was between 33.60 ~ 45.20 at.%. Although amount of the residual brazing filler reaction phase disappeared by prolonging the dwell time, it was still necessary to further increase the brazing temperature for completely eliminating the residual brazing filler reaction phase.

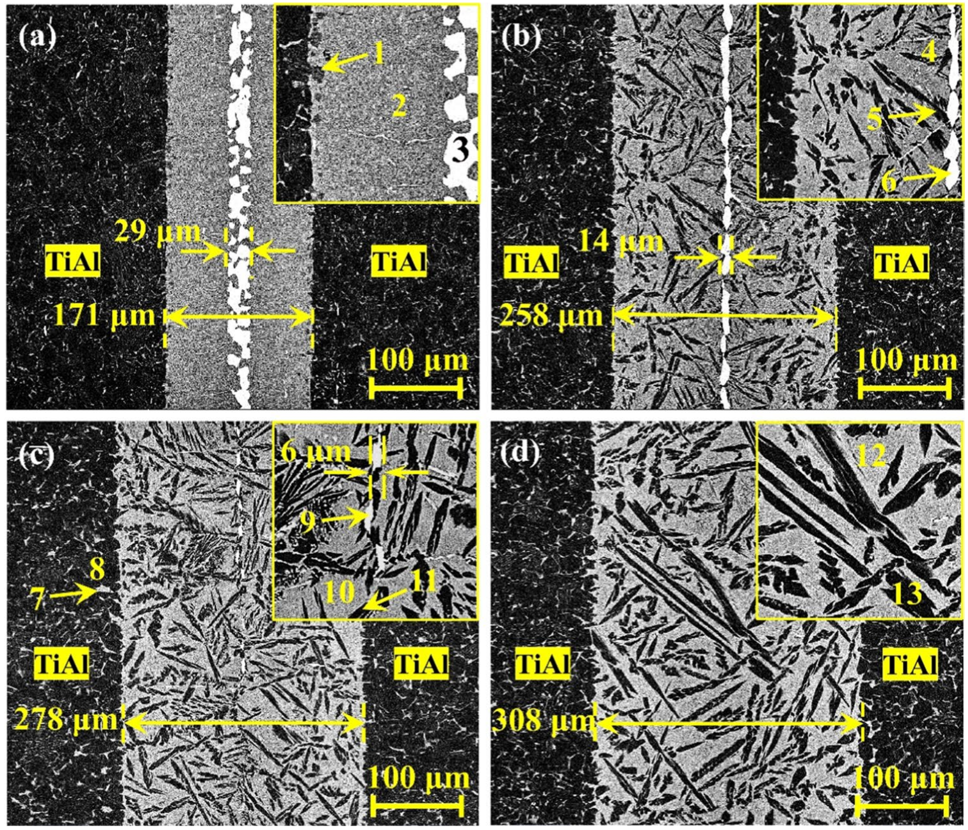

Fig. 4 Backscattered electron images of the TiAl joints brazed at 1140 °C/20 min (**a**), 1180 °C/45 min (**b**), 1180 °C/75 min (**c**), and 1210 °C/45 min (**d**), respectively

On the other hand, with increasing the brazing temperature to 1210 °C, the joint thickness was evidently increased to 308 μm and the size of the lath-like γ-TiAl phase gradually became larger (Fig. 4d). Significantly, this brazing temperature increase almost eliminated the residual brazing filler reaction phase, which might bring potential benefits to the joint strength.

Under the brazing condition of 1210 °C/45 min, the content of the main elements Ti and Al in the brazing seam (microzones "12" and "13" in Fig. 4d) was close to that of the base metal (microzones "7" and "8" in Fig. 4c). As shown in Fig. 6, the elements Ti, Fe, Mn, Ni, and Zr exhibited homogeneous distribution. It seemed that sufficient diffusion within the joint occurred and the

Table 3 EDS analysis results for the microzones marked in Fig. 4

Microzones	Element (at.%)									Deduced phases
	Ti	Al	Fe	Mn	Ni	Nb	Zr	Cr	Ta	
1	56.53	36.30	0.39	0.95	0.26	4.07	0.19	1.03	0.20	γ-TiAl + α_2-Ti_3Al
2	53.92	32.40	3.47	4.18	0.50	3.05	0.75	1.49	0.30	γ-TiAl + α_2-Ti_3Al
3	31.50	34.30	10.40	9.55	4.83	1.46	6.52	1.43	0.00	Residual brazing filler reaction phase
4	54.37	33.45	2.87	3.94	0.32	2.73	0.62	1.55	0.15	γ-TiAl + α_2-Ti_3Al
5	48.62	44.12	1.29	1.59	0.27	2.77	0.73	0.52	0.09	γ-TiAl
6	29.65	40.93	7.13	7.22	5.65	2.06	5.41	1.82	0.13	Residual brazing filler reaction phase
7	53.24	33.50	1.88	2.18	0.62	4.34	0.09	3.77	0.40	γ-TiAl + α_2-Ti_3Al
8	46.90	46.80	0.13	0.05	0.07	4.36	0.24	1.31	0.10	γ-TiAl
9	31.58	39.40	7.77	6.55	4.58	2.81	5.07	2.22	0.10	Residual brazing filler reaction phase
10	54.24	33.60	2.73	3.54	0.55	2.89	0.47	1.77	0.20	γ-TiAl + α_2-Ti_3Al
11	47.56	45.20	1.13	1.32	0.23	2.90	0.71	0.75	0.20	γ-TiAl dissolved with of Fe-Mn-Nb elements
12	52.45	34.00	3.24	3.91	0.74	3.02	0.40	2.07	0.17	γ-TiAl + α_2-Ti_3Al
13	47.98	45.34	0.86	1.45	0.27	2.96	0.36	0.60	0.18	γ-TiAl dissolved with of Fe-Mn-Nb elements

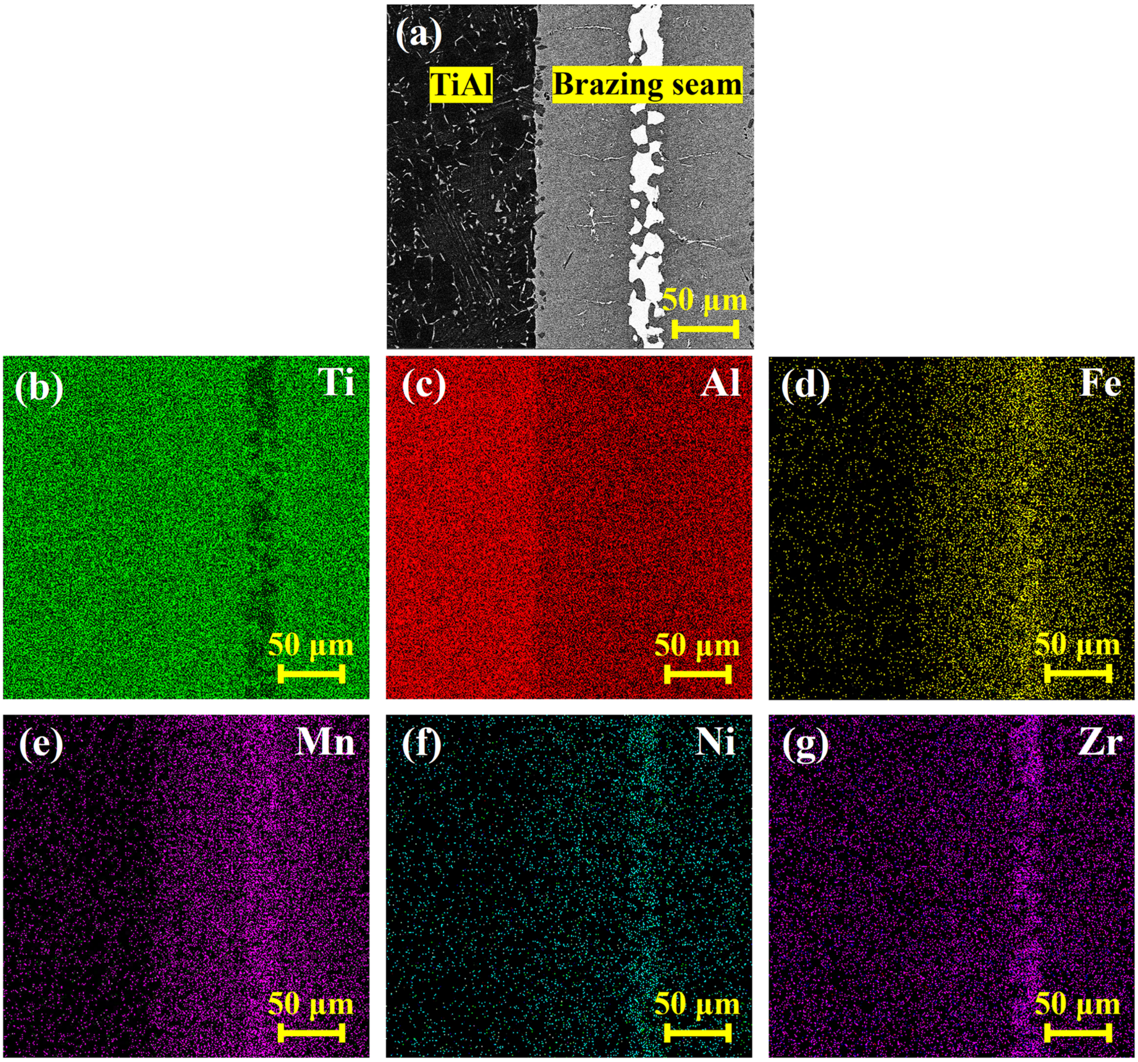

Fig. 5 Backscattered electron images of magnified morphology for the joint brazed at 1140 °C/20 min (**a**), and area distribution map of elements Ti (**b**), Al (**c**), Fe (**d**), Mn (**e**), Ni (**f**), Zr (**g**)

overall composition of the joint was characterized by 47.98 ~ 52.45 at.% Ti, 34.00 ~ 45.34 at.% Al, 0.86 ~ 3.24 at.% Fe, 1.45 ~ 3.91 at.% Mn, 0.27 ~ 0.74 at.% Ni, and 0.36 ~ 0.40 at.% Zr. In other words, a sound brazing joint can be obtained with the composition close to that of the base metal.

The effect of brazing parameter on the area percentage of γ-TiAl phase within the brazed joint, the thickness of residual brazing filler reaction phase, and the joint thickness is shown together in Fig. 7. On the whole, when the brazing parameter becomes stronger, the joint thickness and the area percentage of γ-TiAl phase wthin the joint increased, and the thickness of residual brazing filler reaction phase decreased. Individually, the new formation of γ-TiAl phase was observed at 1180 °C/45 min and the residual brazing filler reaction phase within the joint almost disappeared at 1210 °C/45 min. Figure 7 also signified that the brazing condition of 1210 °C/45 min caused the maximum joint thickness of 308 μm and the maximum area percentage of γ-TiAl phase of 33.77%, as well as the almost elimination of the residual brazing filler reaction phase.

From the perspective of diffusion mechanism, the diffusivity of alloying elements Fe, Mn, and Ni followed the interstitial diffusion mechanism in α-Ti, which belonged to the faster diffusion elements. On the contrary, Zr element exhibited slow diffusion rate due to its vacancy mechanism [41]. For the brazing parameter of 1140 °C/20 min or 1180 °C/45 min, the residual brazing filler reaction phase remained in the central part of the joint due to its too weak high-temperature diffusion. On the brazing condition of 1210 °C/45 min, it was believed that the sufficient diffusion within the joint occurred. Moreover, the Zr element concentration of 3 ~ 8 wt.% in the brazing alloy was quite low. As a result, the joint composition of 0.86 ~ 3.24 at.% Fe,

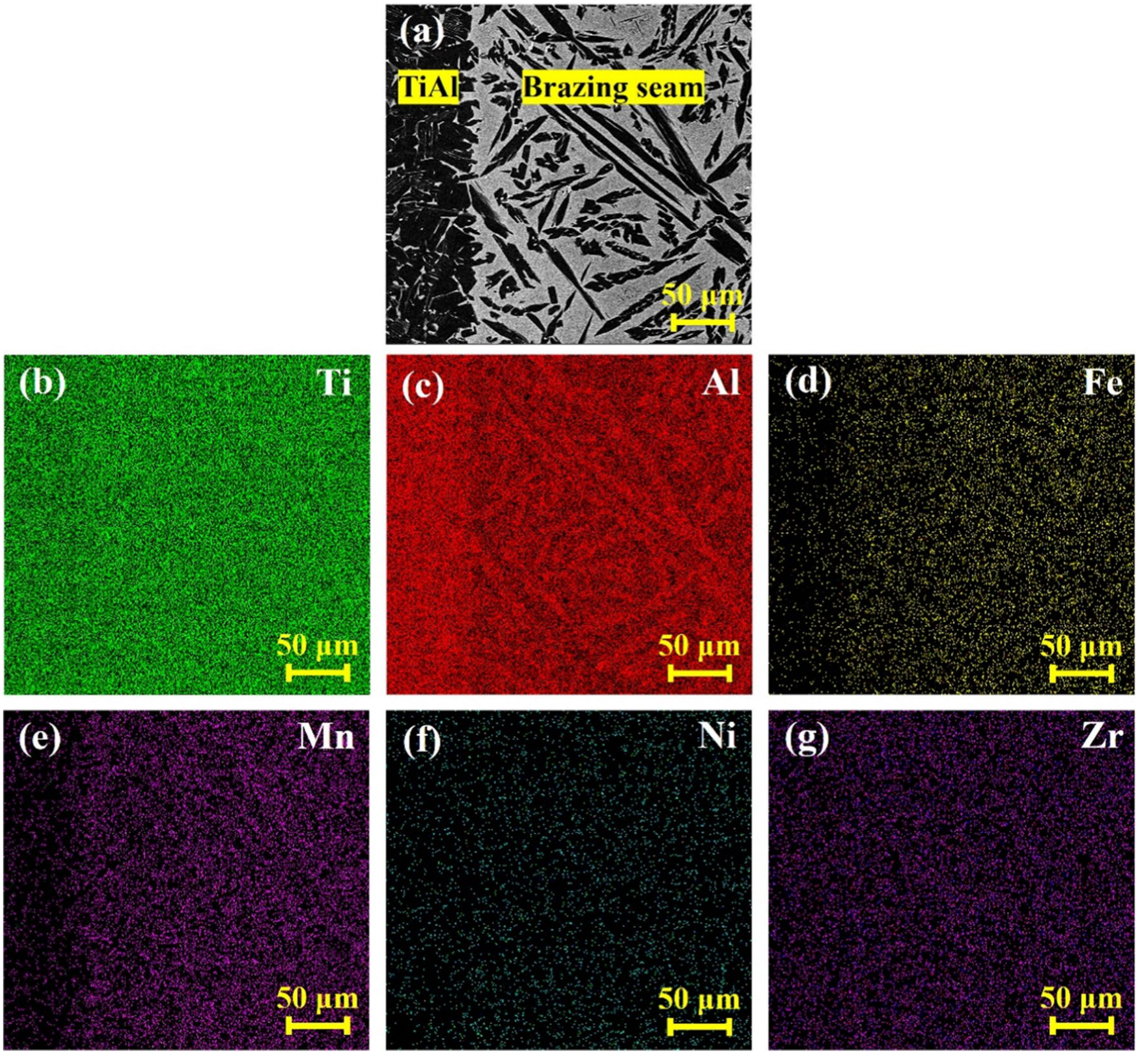

Fig. 6 Backscattered electron images of magnified morphology for the joint brazed at 1210 °C/45 min (**a**), and area distribution map of elements Ti (**b**), Al (**c**), Fe (**d**), Mn (**e**), Ni (**f**), Zr (**g**)

1.45 ~ 3.91 at.% Mn, 0.27 ~ 0.74 at.% Ni, and 0.36 ~ 0.40 at.% Zr exhibited homogeneous distribution and residual brazing filler reaction phase was almost eliminated after the brazing, and this undoubtedly improved the joint strength.

3.3 Mechanical properties of the brazed joints

The effect of brazing parameter on the tensile strength of the brazed joint at room temperature is shown in Fig. 8. With enhancing the brazing parameter, the tensile strength first dramatically increased to 367 MPa at 1180 °C/45 min from 194 MPa at 1140 °C/20 min. Obviously, the diffusion was not sufficient at 1140 °C/20 min, resulting in the thick residual brazing filler reaction phase and the weak joint. The improvement of the tensile strength might be attributed to the strong diffusion behavior of elements and the partial dissolving of the

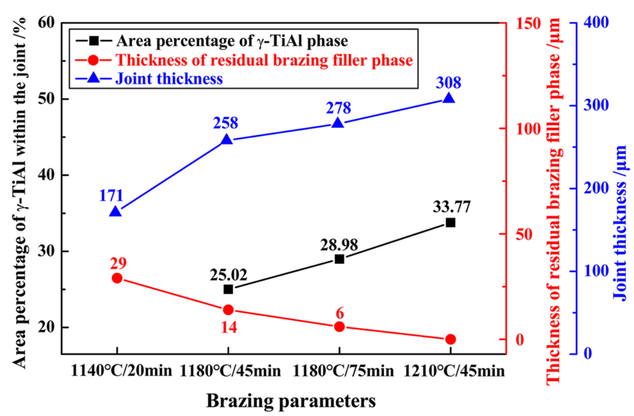

Fig. 7 Effect of brazing parameter on the area percentage of γ-TiAl, the thickness of residual brazing filler reaction phase, and the joint thickness

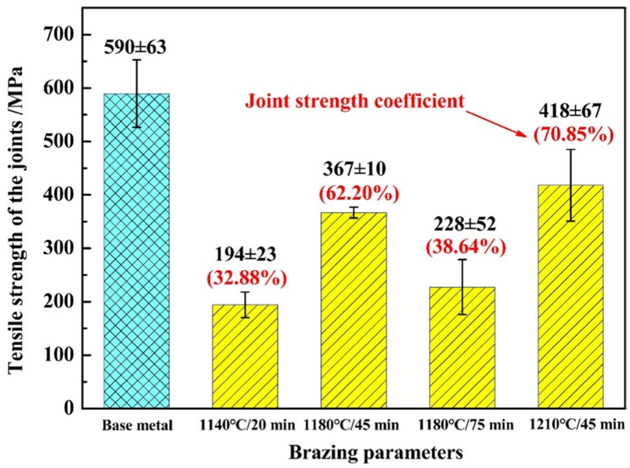

Fig. 8 Effect of brazing parameter on the tensile strength and the joint strength coefficient at room temperature

residual brazing filler reaction phase, as well as the formation of γ-TiAl within the brazed joint. However, the decrease of the tensile strength to 228 MPa under the brazing condition of 1180 °C/75 min was also noticeable, and this might be associated with the microstructure of γ-TiAl phases within the brazing seam and the interface between the brazing seam and the base metal, as shown in Fig. 4c. Finally, the maximum tensile strength of 418 MPa was achieved with the joining parameter of 1210 °C/45 min, which was caused by the almost complete elimination of the residual brazing filler reaction phase and the homogeneous distribution of the main element in the brazing alloy throughout the whole joint, as shown in Fig. 6. Compared with the tensile strength 590 MPa of the parent material, the brazing condition of 1210 °C/45 min offered the highest strength coefficient of 70.85%.

Due to the sufficient diffusion between the brazing seam and the base metal, the Ni concentration within the joint was decreased to the low value of 0.27 ~ 0.74 at.%, and this was favorable to suppress the formation of brittle Ti-Ni intermetallic compounds. Moreover, the dissolved elements of 0.86 ~ 3.24 at.% Fe, 1.45 ~ 3.91 at.% Mn, and 0.36 ~ 0.40 at.% Zr should play an important role of solid solution strengthening, and thus had a beneficial effect on the joint strength [14, 21, 22]. However, it seems that the composition of the brazing filler alloy still needs to be optimized in future for further improvement of the joint strength [16, 19, 28, 42].

The fracture location and the fracture path are shown in Fig. 9. The cracks initiated and propagated at the center of the joint brazed at 1140 °C/20 min and 1180 °C/45 min, indicating that the continuous residual brazing filler reaction phase in the center of the joint caused the formation of cracks. In other words, the residual brazing filler reaction phase was the main factor to the lower strength of the brazed joint. On the contrary, for the joint brazed at 1180 °C/75 min and 1210 °C/45 min, the cracks initiated and propagated at the interface between the brazing seam and the base metal. Due to the fact that the discontinuous residual brazing filler reaction phase in the joint brazed at 1180 °C/75 min was

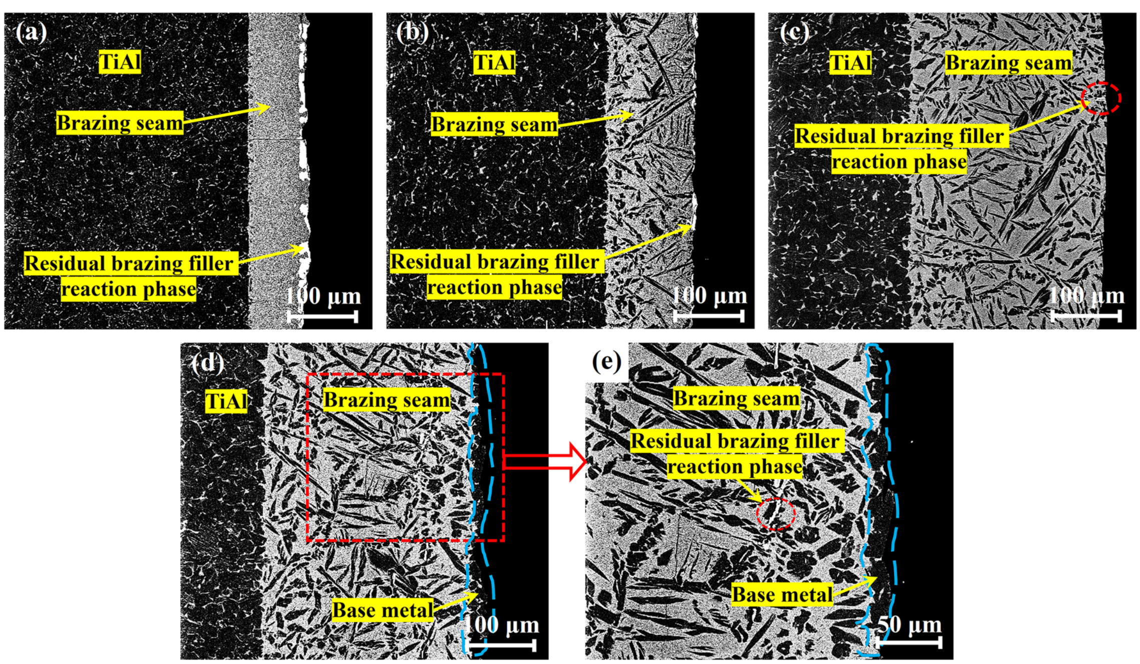

Fig. 9 Fracture paths of the joints brazed at 1140 °C/20 min (**a**), 1180 °C/45 min (**b**), 1180 °C/75 min (**c**), 1210 °C/45 min (**d**), and the magnified morphology of the red dash rectangle zone (**e**)

thin and remained in small amount (shown in Fig. 9c), the tensile test specimen fractured at the interface. In this case, the detrimental effect of the residual brazing filler reaction phase on joint strength might be weakened.

Different from the joint brazed at 1180 °C/75 min, the fracture interface obtained by the brazing parameter of 1210 °C/45 min displayed far less smoothness and contained a small quantity of base metal, as shown in Fig. 9d. The roughened interface might be attributed to the stronger dissolution of TiAl and the more sufficient interdiffusion between the TiAl base metal and the brazing seam. Indeed, the adhered TiAl base metal at the fracture interface inferred that a strong metallurgical bonding between the brazing seam and the base metal had been formed and the strength of the brazing seam was comparable to that of base metal. The mixed fracture path passing through the base alloy and the brazing seam is shown in Fig. 9e. The fracture behavior exhibited a mixed-mode of intergranular and transgranular fracture. This fracture mode should be favorable to the improvement of the joint strength.

4 Conclusions

The main conclusions of the present study can be summarized as follows:

1 The Ti-(18 ~ 24)Mn-(12 ~ 18)Fe-(3 ~ 8)Ni-(3 ~ 8)Zr (wt.%) medium-entropy filler alloy was proposed for TiAl joining, and the joints brazed at 1210 °C/45 min exhibited the maximum room-temperature tensile strength of 418 MPa, the highest joint strength coefficient of 70.85%.

2 The brazed joint was composed of γ-TiAl, α_2-Ti_3Al, and residual brazing filler reaction phase. Under the brazing condition of 1210 °C/45 min, a sound joint was achieved with a desirable composition characterized by 0.86 ~ 3.24 at.% Fe, 1.45 ~ 3.91 at.% Mn, 0.27 ~ 0.74 at.% Ni, and 0.36 ~ 0.40 at.% Zr.

3 The joint brazed at 1210 °C/45 min offered the maximum joint thickness of 308 μm and the maximum area percentage of γ-TiAl phase of 33.77%, as well as the almost complete elimination of residual brazing filler reaction phase.

4 Under the brazing condition of 1140 °C/20 min and 1180 °C/45 min, the joint fractured along the residual brazing filler reaction phase in the center of the brazed joint. Differently, the joint brazed at 1180 °C/75 min and 1210 °C/45 min fractured at the interface between the brazing seam and the base metal, and the joint fracture showed a mixed-mode of intergranular and transgranular fracture.

Funding This research was supported by the National Natural Science Foundation of China under Grant Nos. 51804286, 51705489, and 52201050.

Data availability No data was used for the research described in the article.

Declarations

Conflict of interest The authors declare no competing interests.

References

1. Perrut M, Caron P, Thomas M, Couret A (2018) High temperature materials for aerospace applications: Ni-based superalloys and γ-TiAl alloys. C R Phys 19:657–671. https://doi.org/10.1080/09603409.2016.1206294
2. Wu XH (2006) Review of alloy and process development of TiAl alloys. Intermetallics 14:1114–1122. https://doi.org/10.1016/j.intermet.2005.10.019
3. Bewlay BP, Nag S, Suzuki A, Weimer MJ (2016) TiAl alloys in commercial aircraft engines. Mater High Temp 33(4–5):549–559. https://doi.org/10.1080/09603409.2016.1183068
4. Clemens H, Mayer S (2013) Design, processing, microstructure, properties, and applications of advanced intermetallic TiAl alloys. Adv Eng Mater 15(4):191–215. https://doi.org/10.1002/adem.201200231
5. Rastkar AR, Sohi MH (2020) Phase identification and fracture strength of plasma brazed joints of Ti-45Al-2Nb-2Mn-1B with Ti-Ni-Cu filler metals. Mater Lett 286:129249. https://doi.org/10.1016/j.matlet.2020.129249
6. Mishra S, Sharma A, Jung DH, Jung JP (2020) Recent advances in active metal brazing of ceramics and process. Met Mater Int 26:1087–1098. https://doi.org/10.1007/s12540-019-00536-4
7. Abbasi M, Bagheri B, Sharifi F, Abdollahzadeh A (2021) Friction stir vibration brazing (FSVB): an improved version of friction stir brazing. Weld World 65:2207–2220. https://doi.org/10.1007/s40194-021-01173-5
8. Tillmann W, Ulitzka T, Wojarski L, Manka M, Ulitzka H, Wagstyl D (2020) Development of high entropy alloys for brazing applications. Weld World 64:201–208. https://doi.org/10.1007/s40194-019-00824-y3
9. Kokabi D, Kaflou A (2021) TiAl/IN718 dissimilar brazing with TiZrNiCuCo high-entropy filler metal: phase characterization and fractography. Weld World 65:1189–1198. https://doi.org/10.1007/s40194-021-01075-6
10. Jöckel A, Baumgartner J, Tillmann W, Bültena J, Bobzin K, Heinemann H, Hebing J, Erck M (2022) Influence of brazing process and gap size on the fatigue strength of shear and peel specimen. Weld World 66:1941–1955. https://doi.org/10.1007/s40194-022-01304-6
11. Shiue RK, Wu SK, Chen SY (2003) Infrared brazing of TiAl intermetallic using BAg-8 braze alloy. Acta Mater 51(7):1991–2004. https://doi.org/10.1016/S1359-6454(02)00606-7
12. Li XQ, Li L, Hu K, Qu SG (2015) Vacuum brazing of TiAl-based intermetallics with Ti-Zr-Cu-Ni-Co amorphous alloy as filler metal. Intermetallics 57:7–16. https://doi.org/10.1016/j.intermet.2014.09.01
13. Ren XY, Ren HS, Kang YW, Xiong HP, Pei C, Chen B, Cheng YY, Ustinov AI (2019) Solid-state diffusion bonding of Nb_{SS}/Nb_5Si_3 composite using Ni/Al and Ti/Al nanolayers. Acta Metall Sin-Engl 32:1142–1150. https://doi.org/10.1007/s40195-019-00906-2

14. Ren HS, Xiong HP, Chen B, Pang SJ (2015) Vacuum brazing TiAl to Ti_3Al using two Ti-based filler metals. Weld World 59(5):639–646. https://doi.org/10.1007/s40194-015-0239-y
15. Shang YL, Ren HS, Jing YJ, Xiong HP, Chen B (2019) Vacuum brazing of TiAl-based alloy using Ti-Zr-Fe filler metal. Weld World 63(5):1461–1467. https://doi.org/10.1007/s40194-019-00759-4
16. Ren HS, Shang YL, Ren XY, Jing YJ, Xiong HP, Cheng YY (2022) Microstructure and mechanical properties of TiAl/TiAl joints brazed with a newly developed Ti-Ni-Nb-Zr quaternary filler alloy. Prog Nat Sci-Mater 32(6):758–768. https://doi.org/10.1016/j.pnsc.2022.07.006
17. Ren XY, Ren HS, Shang YL, Xiong HP, Zhang K, Zheng JH, Liu D, Lin JG, Jiang J (2020) Microstructure evolution and mechanical properties of Ti_2AlNb/TiAl brazed joint using newly-developed Ti-Ni-Nb-Zr filler alloy. Prog Nat Sci-Mater 30(3):410–416. https://doi.org/10.1016/j.vacuum.2023.112365
18. Jing YJ, Xiong HP, Shang YL, Ren XY (2021) Interfacial microstructure and tensile strength of TiAl joint brazed with an improved Ti-Zr-Cu-Ni filler. Weld World 65(7):1–8. https://doi.org/10.1007/s40194-020-01015-w
19. Shang YL, Ren XY, Ren HS, Pang SJ, Jing YJ, Cheng YY, Xiong HP (2022) Effect of element Zr in Ti-Zr-Ni-Nb system brazing filler alloys on the microstructure and strength of TiAl/TiAl joints. Weld World 66(7):1437–1446. https://doi.org/10.1007/s40194-022-01274-9
20. Herziga C, Przeorskia T, Frieselb M, Hiskera F, Divinski S (2001) Tracer solute diffusion of Nb, Zr, Cr, Fe, and Ni in γ-TiAl: effect of preferential site occupation. Intermetallics 9(6):461–472. https://doi.org/10.1016/S0966-9795(01)00025-5
21. Liu B, Liu Y, Qiu CZ, Zhou CX, Li JB, Li HZ, He YH (2015) Design of low-cost titanium aluminide intermetallics. J Alloy Compd 640:298–304. https://doi.org/10.1016/j.jallcom.2015.03.239
22. Motha S, Maledi N, Tlotleng M (2022) Characterization of Mn micro alloyed TiAl fabricated using laser engineered net shaping (LENS). Mater Today: Proc 640:298–304. https://doi.org/10.1016/j.matpr.2022.04.817
23. Villars P, Prince A, Okamoto H (1995) Handbook of ternary alloy phase diagrams. ASM International, New York
24. Massalski TB (1992) Alloy phase diagrams binary alloy phase diagrams. ASM International, New York
25. Ren HS, Feng HL, Ren XY, Pang SJ, Cheng YY, Xiong HP (2022) Joining of TiAl-based alloy and a Ni-based superalloy with a NiCoFeCuSiB high entropy filler metal. Weld World 66:557–565. https://doi.org/10.1007/s40194-021-01245-6
26. Hardwick L, Rodgers P, Pickering E, Goodall R (2021) Development of a novel Ni-based multi-principal element alloy filler metal, using an alternative melting point depressant. Metall Mater Trans A 52(6):2534–2548. https://doi.org/10.1007/s11661-021-06246-0
27. Cai YS, Liu RC, Ji HB, Cui YY, Yang R (2021) Vacuum brazing TiAl-based intermetallics using novel Ti-Fe-Mn eutectic brazing alloy. Intermetallics 136:107274. https://doi.org/10.1016/j.intermet.2021.107274
28. Song XG, Cao J, Liu YZ, Feng JC (2012) Brazing high Nb containing TiAl alloy using TiNi-Nb eutectic braze alloy. Intermetallics 22:136–141. https://doi.org/10.1016/j.intermet.2011.10.020
29. Ren XY, Liu W, Ren HS, Jing YJ, Mao W, Xiong HP (2020) Microstructures and joining characteristics of Nb_{SS}/Nb_5Si_3 composite joints by newly-developed Ti66-Ni22-Nb12 filler alloy. J Mater Sci Technol 58:95–99. https://doi.org/10.1016/j.jmst.2020.03.047
30. Ren XY, Xiong HP, Kang YW, Pei C, Chen B, Cheng YY (2019) Microstructure and mechanical properties of vacuum brazed Nb_{SS}/Nb_5Si_3 composite joints using Ni-based filler alloys. Metall Mater Trans A 50:5181–5190. https://doi.org/10.1007/s11661-019-05435-2
31. Ren HS, Xiong HP, Ye L, Ren XY, Li WW, Qin RY (2021) Microstructures and mechanical properties of TiAl/Ni-based superalloy joints brazed with Fe-based filler metal. Weld World 65:79–85. https://doi.org/10.1007/s40194-020-00998-w
32. Srivatsan TS, Gupta M (2020) High entropy alloys: innovations, advances, and applications, 1st edn. CRC Press, Florida
33. Yang W, Pang SJ, Wang G, Liu Y, Liaw PK, Zhang T (2022) Ti-Zr-Hf-Nb-Ta-Sn high-entropy alloys with good properties as potential biomaterials. Rare Met 41:2305–2315. https://doi.org/10.1007/s12598-021-01938-3
34. Takeuchi A, Inoue A (2005) Classification of bulk metallic glasses by atomic size difference, heat of mixing and period of constituent elements and its application to characterization of the main alloying element. Mater Trans 46(12):2817–2829. https://doi.org/10.2320/matertrans.46.2817
35. Biswas K, Gurao NP, Maiti T, Mishra RS (2022) High entropy materials processing, properties, and applications. Springer Nature Singapore Pte Ltd., Singapore
36. Ohnuma I, Fujita Y, Mitsui H, Ishikawa K, Kainuma R, Ishida K (2000) Phase equilibria in the Ti-Al binary system. Acta Mater 48(12):3113–3123. https://doi.org/10.1016/S1359-6454(00)00118-X
37. Schuster JC, Palm M (2006) Reassessment of the binary aluminum-titanium phase diagram. J Phase Equilib Diff 27(3):255–277. https://doi.org/10.1361/154770306X109809
38 Witusiewicz VT, Bondar AA, Hecht U, Rex S, Velikanova TY (2008) The Al-B-Nb-Ti system III. thermodynamic re-evaluation of the constituent binary system Al-Ti. J Alloy Compd 465(12):64–77. https://doi.org/10.1016/j.jallcom.2007.10.061
39 Lee SJ, Wu SK, Lin RY (1999) Infrared joining of TiAl intermetallics using Ti-15Cu-l5Ni foil-I. the microstructure morphologies of joint interfaces. Acta Mater 46(4):1283–1295. https://doi.org/10.1016/S1359-6454(97)00298-X
40. Si XQ, Zhao HY, Cao J, Song XG, Tang DY, Feng JC (2015) Brazing high Nb containing TiAl alloy using Ti-28Ni eutectic brazing alloy: interfacial microstructure and joining properties. Mater Sci Eng A 636:522–528. https://doi.org/10.1016/j.msea.2015.03.108
41. Lütjering G, Williams JC (2003) Titanium. Springer Berlin, Heidelberg. https://doi.org/10.1007/978-3-540-71398-2
42. Liu W, Huang S, Ye CT, Jia L, Kang YW, Sha JB, Chen BQ, Wu Y, Xiong HP (2023) Progress in Nb-Si ultra-high temperature structural materials: a review. J Mater Sci Technol 149:127–153. https://doi.org/10.1016/j.jmst.2022.11.022